Egyptian Journal of Chemistry

http://ejchem.journals.ekb.eg/

Cu(II)/Z4A as an Efficient Nanocomposite for Oxidative Degradation of Indole and Optimization of Effective Factors via RSM Procedure

Samira Amiri Khoshkar Vandani[1], Reza Fazaeli[2,*], Masoud Giahi Saravani[1], Hoda Pasdar[4]

[1]Department of Chemistry, South Tehran Branch, Islamic Azad University, Tehran, Iran
[2] Department of Chemical engineering, Faculty of engineering, South Tehran Branch, Islamic Azad University, Tehran, Iran
[3]Department of Chemistry, North Tehran Branch, Islamic Azad University, Tehran, Iran

Abstract

One of the aromatic contaminants in the oil and fuel is indole, which is toxic even at low doses and is considered as air and water pollutant. In this research, the surface of Zeolite 4A (Z4A) was modified by Cu(II)nanoparticles to introduce a desirable nanocomposite (Cu(II)/Z4A) for indole oxidative degradation. The catalysts characterization was carried out by XRD, SEM, EDS, FTIR, and BET/BJH techniques. Response Surface Methodology (RSM) based on Box-Behnken Design (BBD) was employed for studying several effective factors influences in indole oxidation process, including pH, weight percentage of loaded copper (Cu(wt %)), mass of composite, and indole initial concentration (IND concentration). The obtained results by BBD revealed the solution pH was the most pivotal factor in indole oxidative degradation and predicted that under the optimum experimental conditions, the efficiency should be 98.91%. Moreover, GC-mass analysis was applied for evaluating side products, of which results led to some mechanisms and new productions to be found by using indole oxidative degradation. The results also demonstrated that due to indole oxidation and applying the proper solvent (ethanol), some side products were generated capable of acting as a fuel octane number enhancer, which may play a significant role in obtaining more valuable fuels.

Keywords: Conversion, Design of Experiments, Isotherm, Zeolite.

1. Introduction

Crude oil consists of different nitrogen and sulfur contents, the major factors of undesirable phenomena, such as air pollution and acidic rain. These phenomena are widely blamed for causing serious threats for the health of all species on the earth; thus, researchers are challenging vigorously to find out more efficient approaches for removing these compounds from the oil cuts [1, 2]. One of these compounds, indole, is containing nitrogen, which produces nitrogen oxides (NO_X) when burned for industrial purposes, and is dispersed into the environment in different ways such as burning fossil fuels and some other industrial activities [3-5]. Furthermore, indole and its derivatives have been regarded as one of the most crucial obstacles for the oxidative desulfurization process for two main reasons [6, 7]. First, since the nitrogen in indole is virtually free, it can interact easily with oxygen; however, that of sulfur due to being strongly bonded

in the heterocycle resonance cannot do it with ease. Second, the products resulting from nitrogen oxidation block the accessible sites of catalysts; thus, it is relatively arduous for sulfur materials to achieve such active sites. In other words, nitrogen compounds poison the active sites of catalysts and reduce the yield of the desulfurization process [8]. Due to these problems, several studies have been carried out to discover a more proper method for removing indole from the environment, like bio-degradation of indole which was conducted through applying different approaches by several researchers [9-12]. The other instance is Hartman *et al.* researches which investigated the method of using heterogeneous biocatalysts through immobilization of CPO and GO_X on SBA-15 [13, 14]. Besides, Ahmed *et al.* studied the adsorption of indole over metal-organic frameworks, which was improved by amino-functionalized MOFs [15]. Zhang *et al.* Also worked on the dearomatization of indole via palladium-

_____

catalyzed allylic C-H activation and could obtain a relatively high efficiency [16]. Nevertheless, these methods and other common approaches for removing nitrogen and sulfur from heterocycle compounds are relatively expensive with low efficiency. For instance, as the operations of such processes require harsh conditions, including high pressure and temperature, providing these circumstances not only diminishes the lifetime of the catalysts but also wastes a huge amount of energy. Therefore, designing a suitable catalyst for indole purification is necessary. One of the recent ways for creating such a design is fixing photocatalysts on the surface of zeolites which has been providing an excellent opportunity for improving zeolites efficiency [17-19]. For instance, in an experimental study, Mihajlovic *et al.* modified natural zeolite with Fe(III), and found that this way increased the adsorption capacity of the zeolite [20]. This method has proved to be quite beneficial for two major reasons. First and foremost, it makes the separation of the designed composite from the reaction solution extremely easier; thus, it makes them reusable for several times. Furthermore, the uniform distribution of the photocatalysts on the surface of mesoporous materials prevents an undesirable phenomenon, known as catalyst agglomeration. There are some notable advantages of applying zeolites for industrial activities, particularly in oil purification. The most remarkable ones are workability under normal conditions, selectivity because of pore size, large specific surface, easy synthesis, and application [21, 22]. One of the zeolite kinds, zeolite 4A (Z4A) from the LTA family, has a three-dimensional framework, which is formed by tetrahedral (Si, Al) O_4 and connected with oxygen vertices creating the channels of zeolite. With its pore size, about 1-14 nm, and its Si/Al ratio, almost 1, Z4A is an operational molecular sieve. In Z4A, the negative charge, produced by isomorphous substitution, is balanced by water molecules and exchangeable cations. Z4A and its composites have been employed in a huge range of laboratory and industrial applications, such as adsorption, ion exchange, and water treatment because of its inexpensive price and reusability [23, 24]. In current study, for loading Cu(II)nanoparticles on the Z4A surface, a facile method is reported. By applying the RSM procedure the influence of several effective factors, including pH, Cu(wt %), IND concentration (mg/L), and the mass of composite (g), is investigated. The side-products are also detected by GC-mass analysis. Finally, the isotherm of the reactions is studied by various isothermic equations.

2. Materials and Methods
2.1. Materials

Indole (C_8H_7N), ethanol (C_2H_5OH), sodium hydroxide (NaOH), hydrochloric acid (HCl), and copper(II) chloride ($CuCl_2.2H_2O$) were purchased from Merck, Germany. Zeolite 4A with the purity of (98%) and the following chemical formula ($Na_{12}Al_{12}Si_{12}O_{48}$) was also purchased from Paksan Co. Iran.

2.2. Preparation of Cu(II)/Z4A Nanocomposite

For synthesizing the Cu(II)/Z4Ananocomposite, a one-step method was applied. For obtaining different Cu(II) weight percentages, 10 mL of three solutions, including various amounts of copper(II) chloride, were prepared and placed inside separate containers; each container containing 1g Z4A. Such containers were shaken for 24h so that Cu(II) particles would disperse entirely on the surface of Z4A. Next, the obtained suspensions were filtered, and then, placed in an oven with 120 °C temperature for at least 5h, to the point that they would completely dry. Finally, for calcination of the resulting composites, the obtained powder was placed in a furnace at 400 °C for 3h.

2.3. Oxidation Procedure

For evaluating the efficiency of the indole oxidation via the prepared nanocomposites, some solutions, including various initial concentrations of indole, were prepared, and ethanol was used as solvent in all solutions. Then, the various amounts of the synthesized composites with different weight percentages of Cu(II), were added to the prepared solutions. The pH of these created suspensions was adjusted with aqueous solutions of NaOH 0.2 M and HCl 0.2 M. Then, the prepared suspensions were shaken in a reactor under UV-C light (64 W) irradiation at room temperature. After 40 min, the samples were centrifuged for 10 min at 15000 (rpm) for composites separation. For calculating the efficiency of oxidation reaction, the absorption of the degradation solutions via the previous steps and that of the same solutions before degradation were evaluated by UV-Vis spectroscopy at $\lambda = 287$ *nm*. The efficiency of the process was determined according to the following equation:

$$Efficiency = \frac{A_0 - A_f}{A_0} \times 100 \qquad (1)$$

Where A_0 and A_f represent the initial and final UV absorbance of the examined solutions [25].

2.4. Design of Experiments (DOE)

The purpose of design of experiments (DOE) method is to obtain reliable and appropriate results based on a limited number of observations. From the design and analysis tools of the experiments, in the design of experiments, methods such as the complete factorial method, the Latin square method, are used in the field of analysis of variance tests and its derivatives, and

_____

regression analysis is one of the most important tools [25-28]. In this research, the Design Expert Software (Version 11.0.3) was used for designing the experiments, and the RSM procedure was employed for determining the role of some influential parameters, four crucial factors, including pH, Cu(wt %), IND concentration (mg/L), and the mass of composite (g), were considered. Also, the possible influences of each parameter on the other parameters were considered. To investigate the influence of each of these introduced factors on the yield of indole oxidation, a valid range of levels for each factor was determined by some initial experiments, resulted in finding a suitable range of levels for each factor, as listed in Table 1. Then, these appropriate levels were given to the DOE software. Among the possible methods of DOE, the BBD method was applied, particularly due to considering the instability and sensitivity of obtained data. Moreover, this method took every sensitiveness and error in the tested parameters into account as a block. Based on the number of factors and their related levels alongside with the response surface levels, five blocks were introduced to the software to achieve more accurate results [29]. Although this increased the number of experiments, it enhanced the obtained results validity. After entering the declared factors and their related levels as well as considered blocks, the software suggested 85 testes to be performed.

Table 1. Studied factors and their levels in the experiments.

Factors	Levels
pH	3, 7, 11
Cu(wt %)	0.01, 0.205, 0.4
Mass of composite (g)	0.004, 0.006, 0.008, 0.01, 0.12
IND concentration (mg/L)	2, 17, 32

2.5. Isothermic Studies

In this study, two-parameter, three-parameter, and four-parameter isotherm models were employed. All utilized models and their related equations, parameters, and constants have been discussed by Saadi *et al.* [30]. Hence, 0.02 g of the composite was added to several containers, including 100 mL of indole with various IND concentrations (between 10 and 100 mg/L), and the pH of solutions in the containers was adjusted to 7. Then, the containers were irradiated with UV-C light in a reactor. After 1h, the final concentration of indole was calculated. The adsorption capacity q_e(mg/g) of the nanocomposite was evaluated by applying Equation (2):

$$q_e = \frac{(C_0 - C_e)V}{W}$$ (2)

Where V is the volume of solution (L), W represents the mass of composite (g), C_0 denotes the initial concentration, and C_e is the final concentration of the indole (mg/L) [31].

3. Results and Discussion
3.1. Characterization

3.2 XRD analysis

Z4A and the prepared composite were characterized by X-ray diffraction (XRD) technique. As observed in Fig. 1, the existence of some sharp peaks showed the high crystallinity of the catalysts. It was also detected that the crystal system of both Z4A and Cu(II)/Z4A nanocomposite was cubic. The appearance of some peaks at 2θ=7.24, 10.28, 12.51, 27.16, 30.168, 34.19, and 52.54° corresponded with the reference code: (00-011-0589). The Miller index associated with each peak ofZ4A was also illustrated in Fig.1. Moreover, after loading Cu(II)nanoparticles, the characteristic peaks shifted to the lower 2θ amounts.
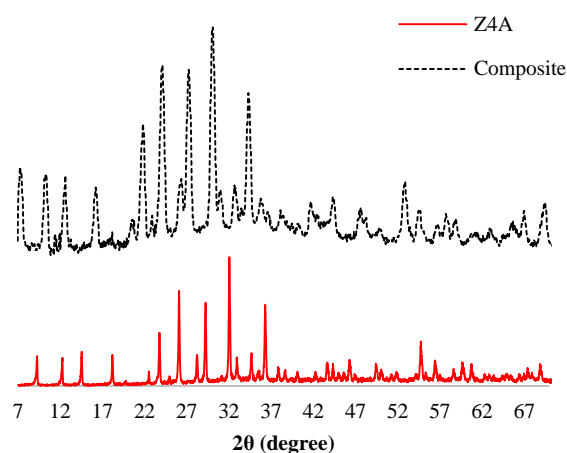

Fig. 1. The XRD patterns.

For calculating the crystallite size of the prepared nanocomposite, the Debye-Sherer equation (3) was used [32].

$$B = \frac{k\lambda}{L cos\theta}$$ (3)

Where β denotes the crystallite size, K is a constant which is usually considered to be 0.89, λ depends on the wavelength of the employed cathode, L denotes the full-width-at-half- maximum (FWHM), and θ is the related angle of the studied peak. Using this equipment, the crystallite size of Z4A was calculated from 80.01nm to 390.79 nm approximately. Furthermore, the average size of the crystallites was around 180.52 nm. However, after loading Cu(II) nanoparticles upon it, the size of crystals in the nanocomposite increased slightly, between 90.3 nm and 420.1 nm with an average size of about 190.8 nm.

3.3. SEM and EDS Analysis

The surface morphology and size of samples were evaluated via scanning electron microscopy (SEM). As displayed in Fig. 2a, SEM revealed the average

diameter of Z4A particles was less than 1 μm. Besides, the samples were composed of regular and cubic elements with a virtually uniform size. Moreover, it demonstrated some bright points in Fig. 2b, referring to Cu(II) nanoparticles, which were distributed properly on the Z4A surface. As shown in Fig. 2c, the energy dispersive X-ray spectrum (EDS) of nanocomposite reveals the presence of Cu(II) particles. Also, the weight percentage of each contained element was as follows: Si(15.65%), O(45.39%), Al(14.18%), and Cu(24.77%).
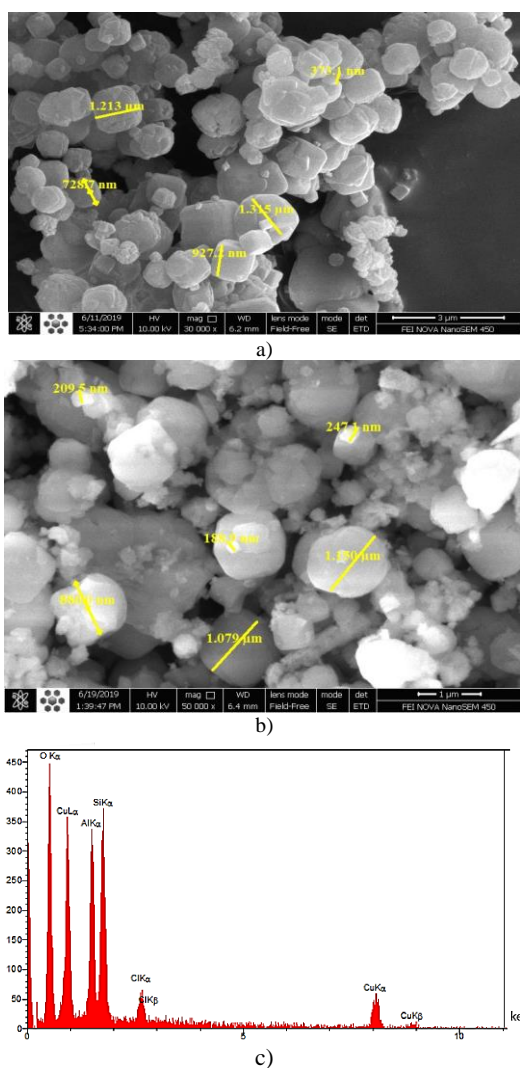

a)

b)

c)

Fig. 2. SEM micrographs of a) Z4A, and b) composite, and c) EDS spectrum of the composite.

3.4. FTIR Analysis

To investigate the chemical properties of the samples, Fourier transform infrared (FTIR) spectroscopy (Bruker, Tensor 27, and Equinox 55) was applied. As depicted in Fig. 3, the presence of a band at 3431.70 cm^{-1} was attributed to the stretching vibration of O-H. For Z4A, the bond of the stretching vibration of Si-O at 1006.62 cm^{-1} and that of the bending vibration of

Si-O-Al at 466 cm^{-1} were its major characteristic ones [33]. Considering the nanocomposite spectra, it seems that the chemical structure of Z4A did not change significantly after loading Cu(II); however, the emergence of a peak at 1383.12 cm^{-1} is associated with forming new bonds after loading the Cu(II) nanoparticles [34].
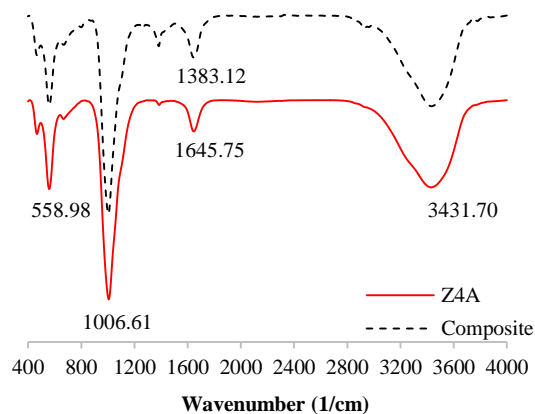

Fig. 3. FTIR spectra of Z4A and Composite.

3.5. BET/BJH Analysis

For determining the surface area and pores size distribution of Z4A and the nanocomposite, the Brunauer-Emmett-Teller (BET) and Barret-Joyner-Halenda (BJH) analyses via a porosity meter (BELSORP Mini II) were employed. The N$_2$ adsorption/desorption isotherm and the pores size distribution of the Z4A were presented in Fig. 4. Relying on the graph, it was realized a B type hysteresis loop formed, indicating incomplete cone-shaped rings [28]. The pattern of pores distribution of Z4A and that of the nanocomposite were evaluated by BJH method. Regarding dv$_P$/dr$_P$ versus r$_p$/nm in the graph, it was understood that although the pores distribution pattern of Z4A did not follow a regular trend, the main condensation of pores occurred at 1-2 nm. In contrast with the previous pattern, that of nanocomposite experienced a virtually constant downtrend.

Table 2. Surface properties of Z4A, and the composite.

Catalyst	a$_{s.BET}$ [m^2 g^{-1}]	Total pore Volume [Cm^{3}g^{-1}]	Mean Pore Diameter (nm)
Z4A	7.007	0.035723	20.393
Cu(II)/Z4A	12.279	0.057232	18.643
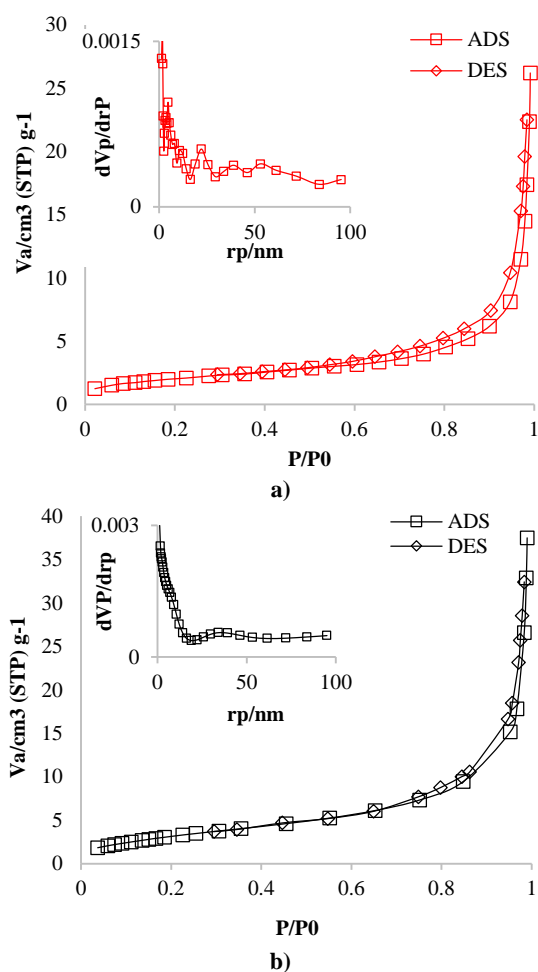
Fig. 4. N_2 Adsorption/ Desorption Isotherm for a) Z4A, and b) The composite.

By investigating all peaks emerging in the GC chromatogram, it was understood that in this photocatalytic reaction, a small percentage of the indole remained unreacted. Besides, there were some other peaks in the GC spectrum, which could be divided into two groups, one of them was noises and GC column contamination (device noise) and the other was side-products generated by indole oxidative degradation and photocatalytic reaction. GC chromatograms in the pre and post-photocatalytic reaction and the five main generated side-products were illustrated in Fig. 5a, b, and c respectively.
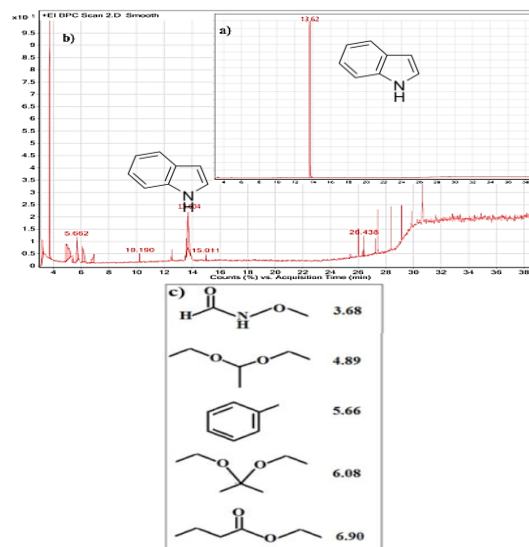

Fig. 5. GC chromatograms of indole a) before reaction, b) after the reaction, and c) main detected side-products.

Table 2, showed the results obtained from BET/BJH technique. According to the table, the surface area and the pore volume had a remarkable increase after loading Cu(II)nanoparticles. In addition, the pore diameter after loading experienced an incidental decline, which meant that Cu(II)nanoparticles loaded on Z4A pores.

3.6. Oxidation Process

The oxidative degradation of indole was examined in detail via the prepared nanocomposite and under UV-C irradiation. By using the UV-C irradiation and the photocatalytic properties of the nanocomposite, an aggressive radical reaction took place, which affected both the pollutant and the solvent (ethanol). This was incredibly great, as no auxiliary oxidants were required. However, in some cases, the adsorption rate of UV-Vis spectrum increased too much and led to negative amounts of efficiency. This meant some side-products were generated which caused impurity for the solvent. As a result, GC-mass spectroscopy was carried out to detect the potential side-products and to determine their reaction pathways.

Two molecules appearing at 4.89 and 6.08 min were apparently 1,1-Diethoxyethane ($C_6H_{14}O_2$) and 2,2-Dimethoxypropane ($C_7H_{16}O_2$) respectively, resulted from the reaction between ethanol and indole photocatalytic degradation side-products. Fig. 6, displayed the possible mechanism of formation of these two side-products. The formation of ketone compounds and their reaction with ethanol led to the formation of acetal groups. Both of these side-products, as oxygenated compounds, could play a similar role as fuel octane number enhancer compounds similar to Methyl tert-butyl ether (MTBE) compound. Hence, ethanol as a solvent not only eliminated indole pollutants but acted as a fuel octane enhancer, which could reduce environmental pollution and produce fuels with higher quality.

The probable mechanisms related to the formation of other side-products in which their peaks were observed at 3.68, 6.90, and 5.66 min, were shown in Fig. 7a, b, and c, respectively. These materials were identified as follows: N-Methoxyformamide ($C_2H_5NO_2$), Toluene (C_7H_8), and Butanoic acid ethyl ester ($C_6H_{12}O_2$) respectively.
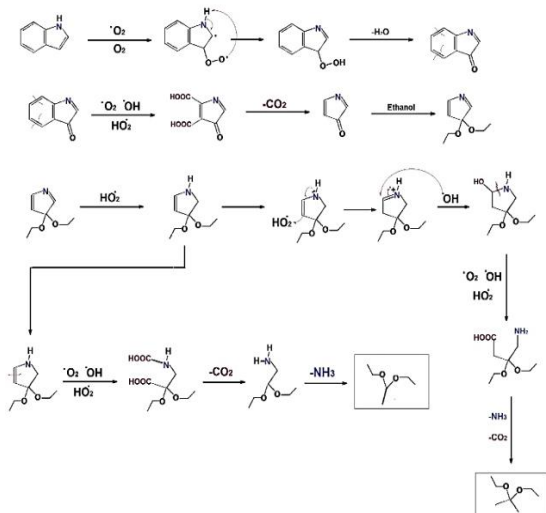
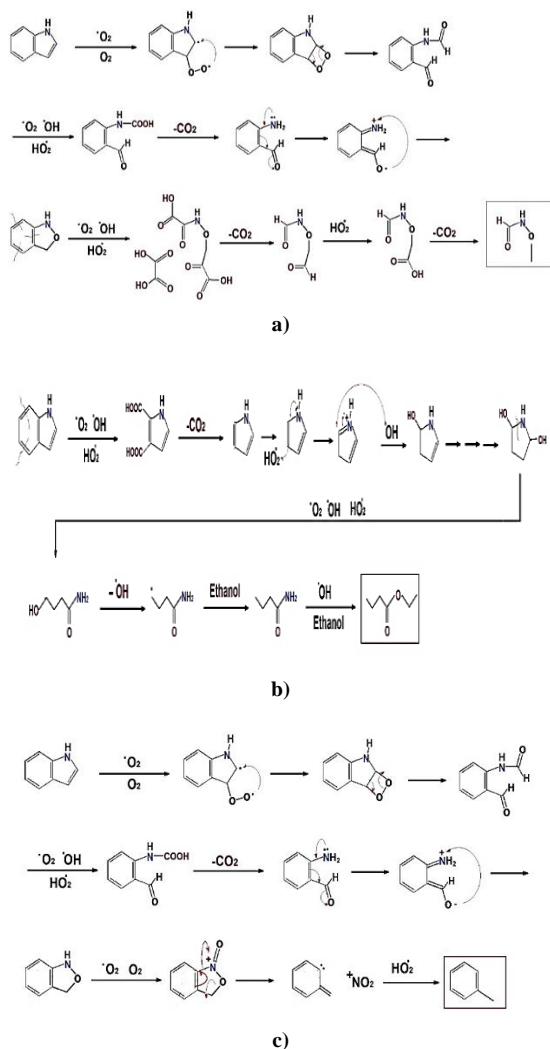Fig. 6. Suggested mechanisms of side-products formed in 4.89 and 6.08 min.

a)

b)

c)

Fig. 7. Suggested mechanism of side-product formed in a) 3.68, b) 6.90, and c) 5.66 min.

3.7. Design of Experiments (DOE)

According to the obtained data after performing all the suggested experiments by DOE, and calculating their efficiency, it was found that the maximum efficiency of the oxidation process(98.60%), occurred in the experiment, in which 0.12 g of composite with Cu(0.205wt %) was added to the reaction solution containing 32 mg/L IND concentration at pH 11. However, in the other experiment, conducted under the same conditions but had a lower amount of IND concentration, the efficiency was calculated to be 31.5%. It could be concluded that a slight decrease in IND concentration has an undesirable effect on the oxidative degradation process. In all experiments, it is very clear that the alkalinity of the medium plays a beneficial role in the oxidation process. In the study on the effect of Cu(wt %), it was observed that an increase in the amount of Cu(wt %), did not have a favorable influence on efficiency. In addition, for investigating the other considered factor, mass of composite, two experiments with the same condition (including pH 11, Cu(0.4 %), and 17 mg/L IND concentration), but containing various amounts of mass of composite (0.12 and 0.004 g, with 23.3 and 19% efficiency respectively) were compared together. It was found that this factor has a direct relationship with efficiency. Concerning the cases mentioned above, it can be concluded that all the given factors, played a crucial role in the oxidation process.

3.8. Statistical analysis

Based on Table 3, the validity of the taken tests based on the RSM model was less than 0.05 (0.0202), suggesting that there was a notable difference between the influence of the variables on the oxidation process. Furthermore, as the F test statistic in the pH variable had a larger number than the other variables, it could be concluded that pH value had the greatest effect on the oxidation process. The standard probability chart showed how the variables followed a normal distribution.

Table 3. ANOVA analysis of the indole oxidation.

ANOVA Response Surface Methodology Cubic Model				
Source	Sum of Squares	Mean Square	F-value	p-value
Model	52534.37	1010.28	1.98	0.0207
A-pH	16503.09	16503.09	32.35	< 0.0001
B-Cu	1511.67	1511.67	2.96	0.0948
C-Pollutant Density	833.75	833.75	1.63	0.2103
D-composite	835.22	208.80	0.4094	0.8005
AB	1254.21	1254.21	2.46	0.1267
AC	48.98	48.98	0.0960	0.7587
AD	1112.29	278.07	0.5452	0.7038
BC	885.51	885.51	1.74	0.1970
BD	3335.88	833.97	1.63	0.1896
CD	940.90	235.22	0.4612	0.7636
A²	581.59	581.59	1.14	0.2936
B²	4219.38	4219.38	8.27	0.0071

C²	8772.43	8772.43	17.20	0.0002
ABC	0.0000			
ABD	1963.16	490.79	0.9622	0.4416
ACD	1674.13	418.53	0.8205	0.5217
BCD	1807.79	451.95	0.8860	0.4834
A²B	571.99	571.99	1.12	0.2975
A²C	1567.75	1567.75	3.07	0.0892
A²D	1167.69	291.92	0.5723	0.6846
AB²	86.79	86.79	0.1701	0.6827
B²D	712.32	178.08	0.3491	0.8427
BC²	0.0000			
C²D	959.70	239.93	0.4704	0.7570
Residual	16322.46	510.08		
Lack of Fit	13994.02	1166.17	10.02	< 0.0001
Pure Error	2328.44	116.42		
Cor Total	68856.83			

In Fig. 8, the normal distribution of variables was shown linearly. Since almost all of the given data were positioned on a normal line, it could be concluded that the statistical population had a normal distribution through the oxidation process. Besides, the normal position of the given data represented the precision of the results obtained via the experiments.
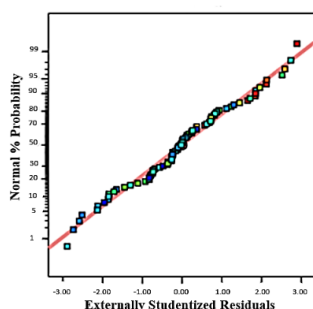

Fig. 8. Scattering diagram of the normal distribution of variables' response.

3.9. Recognition of factors' behavior through the oxidative degradation process

The effects of the studied factors and their behaviors by applying the analyses of three-dimensional graphs could be easily observed.

Based on Fig. 9, at the point of maximum pH, the ratio of efficiency increased considerably. In other words, an increase in the amount of pH had a desirable influence on efficiency. The notable decline in Cu(wt %) and pH showed a decrease in efficiency. This notable finding revealed that in an acidic medium, why efficiency was reduced, which suggested there might be some side-products.
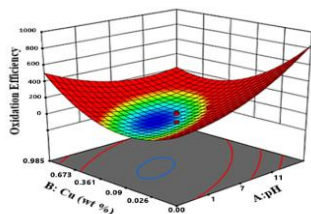

Fig. 9. The three-dimensional diagram of the relationships and influences of the Cu(wt %) and pH on indole oxidation.

As shown in Fig. 10, as the IND concentration increased, the yield diminished. It was observed the

nanocomposite was a preferable catalyst for treating indole at low concentrations. In addition, one of the most crucial findings was the IND concentration and the pH value was related together. In the green parts of the diagram, the efficiency of the oxidation process was grown. Thus, at each IND concentration, the oxidation process could take place by enhancing the alkaline properties of the solution. Besides, findings revealed that at the higher amounts of pH, the oxidation process would occur at all IND concentrations.
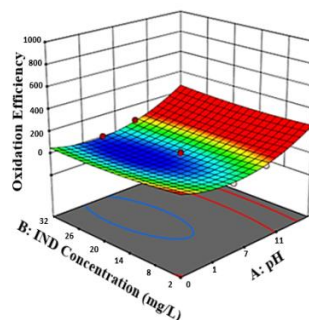

Fig. 10. The three-dimensional diagram of the relationships and influences of the IND concentration and pH on indole oxidation.

The behaviors of two effective variables, including Cu(wt %) and IND concentration, in the performed experiments are shown clearly in Fig. 11. In this diagram, the maximum amount of efficiency is indicated in red colour. By evaluating this chart, it was found that in comparison with IND concentration, changes in Cu(wt %) do not play a substantial role in the oxidation process. However, regardless of IND concentrations, an increase in Cu(wt %) caused an enhancement in the oxidation efficiency.
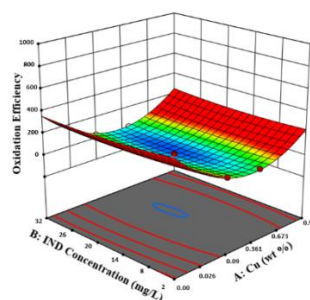

Fig. 11. The three-dimensional diagram of the relationships and influences of the Cu(wt %) and the IND Concentration on indole oxidation.

3.10. Determining the optimal conditions

According to the obtained data through DOE studies, it was clear that all variables in the experiments required replications to optimize the oxidation process. Moreover, by considering the introduced blocks, the optimum circumstances were introduced by the software, which provided on the optimal version of experiments (presented in Table 4). Hence,

_____

it could be predicted that under such conditions, the highest efficiency would be 98.91%. The optimized condition was also employed in an experiment, whereby efficiency of 98.6% was achieved. Besides, the obtained results suggested that there was a significant correlation between theoretical and experimental data.

Table 4. Optimal Version.

pH	Cu (wt.%)	IND Concentration (ppm)	Mass of Composite (g)	Efficiency (%)
11.000	0.010	2.000	0.004	98.91

3.11. Isotherm Results

The isothermic models were fitted by Curve Expert Software, and then, the errors were minimized by MATLAB Software. The models with the highest correlation coefficient are listed in Table 5. The obtained results revealed that the Fritz-Schlunder, a four-parameter model, with the maximum correlation coefficient (0.999) and a small error value (0.075), was in a proper agreement with the obtained experimental data.

Table 5. Isotherms, error minimization, and correlation maximization.

Model	Equation	Correlation Coefficient	Error Value
Fritz-Schlunder	$q_e = \dfrac{C.C_e^{\alpha}}{1 + D.C_e^{\beta}}$	0.9992	0.075772
Sips	$q_e = \dfrac{k_s.a_s.C_e^{B_s}}{1 + a_s.C_e^{B_s}}$	0.9835	0.53691
Koble_Corrigan	$q_e = \dfrac{A.C_e^{n}}{1 + B.C_e^{n}}$	0.9835	1.9913
Hill	$q_e = \dfrac{q_m.C_e^{n_H}}{K_D + C_e^{n_H}}$	0.9835	4.6831
Jossens	$C_e = \dfrac{q_e}{H}.e^{(F.q_e^{p})}$	0.9940	15.328
Fowler_Guggenheim	$C_e = \dfrac{q_e}{K_{FG}.(q_m - q_e)}.exp\left(\dfrac{2.q_e.W}{RTq_m}\right)$	0.9873	15.489
Elovich	$C_e = \dfrac{q_e}{q_m.K_E.exp\left(\dfrac{-q_e}{q_m}\right)}$	0.9919	16.128

4. Conclusion

In this study, Cu(II)nanoparticles were loaded on the Z4A for preparing an economic nanocomposite for indole oxidative degradation. By employing RSM procedure based on BBD design, the role of some crucial factors including pH, Cu(wt %), mass of catalyst, and IND concentration was investigated, and then, the optimum condition was determined. It was found the pH of the medium played the most substantial role in this process. In addition, the proper design of the nanocomposite and the use of UV-C

light made the oxidation reaction occur without using any auxiliary oxidants. For evaluating the generated side-products, GC-mass analysis was used. The obtained results indicated that the major portion of indole converted to five substances. It was also found that applying a suitable solvent caused the generation of some side-products, which could act as fuel octane enhancer compounds similar to how MTBE materials act. It is noteworthy to state that among all studied isotherm equations, the four-parameter isothermic model (Fritz-Schlunder), with the highest correlation coefficient (0.9992) and the lowest error ratio (0.075772) presented the best agreement with the experimental data.

5. References

1. Fard, N. E., Fazaeli, R., Yousefi, M., &Abdolmohammadi, S. Morphology- Controlled Synthesis of CuO, CuO Rod/MWW Composite for Advanced Oxidation of Indole and Benzothiophene. *Chem Select*, **4**(33), 9529-9539 (2019).
2. Prado, G. H., Rao, Y., & de Klerk, A. Nitrogen removal from oil: a review. *Energ Fuel*, **31**(1), 14-36 (2017).
3. Yao, Q., Xu, L., Han, Z., & Zhang, Y. Production of indoles via thermo-catalytic conversion and ammonization of bio-derived furfural. *Chem Eng J*, **280**, 74-81(2015).
4. Xiaojian, Z., Yue, Z., Huan, W., Suxia, Z., &Ruibao, J. Emergent drinking water treatment for taste and odor control in Wuxi City water pollution incident. *Water Wastewater Eng*, 9. (2007).
5. Merabet, S., Bouzaza, A., &Wolbert, D. Photocatalytic degradation of indole in a circulating upflow reactor by UV/TiO₂ process—Influence of some operating parameters. *J Hazard Mater*, **166**(2-3), 1244-1249 (2009).
6. Baskaran, T., Joshi, A., Kamalakar, G., &Sakthivel, A. A solvent free method for preparation of β-amino alcohols by ring opening of epoxides with amines using MCM-22 as a catalyst. *ApplCatal A: Gen*, **524**, 50-55 (2016).
7. ZHOU, X. R., Hong, M. A., FU, X. M., YAO, C. B., & XIAO, J. Q. Catalytic oxidation of carbazole using t-butyl hydroperoxide over molybdenum catalysts. *J Fuel ChemTechnol*, **38**(1), 75-79 (2010).
8. Moghaddam, R. B., & Pickup, P. G. Influences of aniline, carbazole, indole, and pyrrole monomers and polymers on formic acid oxidation at Pt electrodes. *Electrochimica Acta*, **107**, 225-230 (2013).
9. Katapodis, P., Moukouli, M., &Christakopoulos, P. Biodegradation of indole at high concentration by persolvent fermentation with the thermophilic fungus Sporotrichum thermophile. *Int Biodeter Biodegr*, **60**(4), 267-272 (2007).
10. Hammouda, S. B., Adhoum, N., &Monser, L. Chemical oxidation of a malodorous compound, indole, using iron entrapped in calcium alginate beads. *J Hazard Mater*, **301**, 350-361 (2016).
11. Gai, K., Qi, H., Zhang, Y., & Ma, D. Degradation of indole in aqueous solution using contact glow discharge plasma. *J Appl Electrochem*, **40**(3), 615-619 (2010).

_____

12. Liu, Y., Wang, L., Huang, Z., Wang, X., Zhao, X., Ren, Y. & Ma, J. Oxidation of odor compound indole in aqueous solution with ferrate (VI): Kinetics, pathway, and the variation of assimilable organic carbon. *Chem Eng J*, **331**, 31-38 (2018).

13. Jung, D., & Hartmann, M. Oxidation of Indole with CPO and GOx Immobilized on SBA-15. *Stud Surf Sci Catal*, **174**, 1045-1050. (2008).

14. Jung, D., & Hartmann, M. Oxidation of indole with CPO and GOx immobilized on mesoporous molecular sieves. *Catal Today*, **157**(1-4), 378-383 (2010).

15. Ahmed, I., &Jhung, S. H. (2015). Effective adsorptive removal of indole from model fuel using a metal-organic framework functionalized with amino groups. *J Hazard Mater*, **283**, 544-550 (2015).

16. Zhang, H., Hu, R. B., Liu, N., Li, S. X., & Yang, S. D. Dearomatization of Indoles via Palladium-Catalyzed Allylic C–H Activation. *Org Lett*, **18**(1), 28-31 (2016).

17. Boosa, V., Bilakanti, V., Velisoju, V. K., Gutta, N., Inkollu, S., &Akula, V. An insight on the influence of surface Lewis acid sites for regioselective CH bond C3-cyanation of indole using NH4I and DMF as combined cyanide source over Cu/SBA-15 catalyst. *Mol Catal*, **445**, 43-51(2018).

18. Si, J., Li, L., Zhang, Y., Zhou, J. C., & Ouyang, W. Preparation of Novel Complex Nano-Structured Gold Catalyst Au@ TiO2/MCM-22, Characterization, and Remarkably Catalytic Performance for Cyclohexane Oxidation. *Mod Res Catal*, **6**(01), 15 (2017)

19. Nikoorazm, M., Ghorbani-Choghamarani, A., &Khanmoradi, M. Synthesis and characterization of Ni (II)–Vanillin–Schiff base–MCM-41 composite as an efficient and reusable nanocatalyst for multicomponent reactions. *RSC advances*, **6**(61), 56549-56561(2016).

20. Mihajlović, M. T., Lazarević, S. S., Janković-Častvan, I. M., Jokić, B. M., Janaćković, Đ. T., &Petrović, R. D. A comparative study of the removal of lead, cadmium and zinc ions from aqueous solutions by natural and Fe (III)-modified zeolite. *Chem Ind Chem Eng Q*, **20**(2), 283-293(2014).

21. Alotibi, M. F., Alshammari, B. A., Alotaibi, M. H., Alotaibi, F. M., Alshihri, S., Navarro, R. M., & Fierro, J. L. G. ZSM-5 Zeolite Based Additive in FCC Process: A Review on Modifications for Improving Propylene Production. *Catal Sur Asia*, **24**(1), 1-10 (2020).

22. Ismail, A. A., Mohamed, R. M., Ibrahim, I. A., Kini, G., &Koopman, B. Synthesis, optimization and characterization of zeolite A and its ion-exchange properties. *Colloid Surfaces A,* **366**(1-3), 80-87(2010).

23. Hui, K. S., & Chao, C. Y. H. Effects of step-change of synthesis temperature on synthesis of zeolite 4A from coal fly ash. *MicroporMesopor Mater*, **88**(1-3), 145-151(2006).

24. Cui, Y., Zheng, Y., & Wang, W. Synthesis of 4A Zeolite from Kaolinite-Type Pyrite Flotation Tailings (KPFT). *Miner*, **8**(8), 338 (2018).

25. Fard, N. E., &Fazaeli, R. Experimental design study of RB 255 photocatalytic degradation under visible light using synthetic Ag/TiO2 nanoparticles: Optimization of experimental conditions. *Iran J Catal*, **8**(2), 133-141 (2018).

26. Kashi, N., Fard, N. E., &Fazaeli, R. Empirical modeling and CCD-based RSM optimization of Cd (II) adsorption from aqueous solution on clinoptilolite and bentonite. *Russ J ApplChem*, **90**(6), 977-992 (2017).

27. Fard, N. E., &Fazaeli, R. Optimization of Operating Parameters in Photocatalytic Activity of Visible Light Active Ag/TiO2 Nanoparticles. *Russ J Physic Chem A*, **92**(13), 2835-2846 (2018).

28. Fazaeli, R., &Fard, N. E. Desulfurization of Gasoline Fuel via Photocatalytic Oxidation/Adsorption Using NaX Zeolite-Based under Mild Conditions: Process Optimization by Central Composite Design. *Russ J ApplChem*, 93(7), 973-982 (2020).

29. Fard, N. E., Fazaeli, R., Yousefi, M., &Abdolmohammadi, S. Oxidation of carbazole by shape-controllable Cu2O on MWW catalysis. *Appl Physic A*, **125**(9), 632 (2019).

30. Saadi, R., Saadi, Z., Fazaeli, R., &Fard, N. E. Monolayer and multilayer adsorption isotherm models for sorption from aqueous media. *Korean J Chem Eng*, **32**(5), 787-799 (2015).

31. Fard, N. E., Fazaeli, R., &Ghiasi, R. Band gap energies and photocatalytic properties of CdS and Ag/CdS nanoparticles for Azo dye degradation. *Chem Eng Technol*, **39**(1), 149-157 (2016).

32. Kibasomba, P. M., Dhlamini, S., Maaza, M., Liu, C. P., Rashad, M. M., Rayan, D. A., &Mwakikunga, B. W. Strain and grain size of TiO2 nanoparticles from TEM, Raman spectroscopy and XRD: The revisiting of the Williamson-Hall plot method. *Results Phys*, **9**, 628-635 (2018).

33. Wang, P., Sun, Q., Zhang, Y., & Cao, J. Synthesis of Zeolite 4A from Kaolin and Its Adsorption Equilibrium of Carbon Dioxide. *Mater*, **12**(9), 1536 (2019).

34. Khanmoradi, M., Nikoorazm, M., &Ghorbani-Choghamarani, A. Anchoring of Cu (II)–vanillin Schiff base complex on MCM- 41: A highly efficient and recyclable catalyst for synthesis of sulfides and 5-substituted 1H–tetrazoles and oxidation of sulfides to sulfoxides. *Appl Organomet Chem*, **31**(9), 3693 (2017).